Supplement of Earth Syst. Sci. Data, 16, 1283–1300, 2024
https://doi.org/10.5194/essd-16-1283-2024-supplement

Open Access Earth System Science Data

Supplement of

Global datasets of hourly carbon and water fluxes simulated using a satellite-based process model with dynamic parameterizations

Jiye Leng et al.

Correspondence to: Jing M. Chen (jing.chen@utoronto.ca)

1. List of the studied sites in the FLUXNET2015 datasets for site-level estimates of m and V_{cmax}^{25}.

Table S1. Main characteristics and studied periods of flux sites in this study, obtained from https://fluxnet.org/data/fluxnet2015-dataset/

Site Name	IGBP	Year	Lat	Lon
BE-Lon	CRO	2005-2014	50.5516	4.7461
CH-Oe2	CRO	2004-2014	47.2863	7.7343
DE-Geb	CRO	2002-2014	51.1001	10.9143
DE-Kli	CRO	2005-2014	50.8931	13.5224
DE-Seh	CRO	2008-2009	50.8706	6.4497
FI-Jok	CRO	2001	60.8986	23.5135
FR-Gri	CRO	2006-2011	48.8442	1.9519
IT-BCi	CRO	2005-2007, 2013-2014	40.5238	14.9574
IT-CA2	CRO	2012-2014	42.3772	12.0260
US-ARM	CRO	2003--2012	36.6058	-97.4888
US-CRT	CRO	2011-2014	41.6285	-83.3471
US-Tw3	CRO	2014	38.1159	-121.6467
IT-Noe	SH	2004-2014	40.6062	8.1512
US-KS2	SH	2004-2006	28.6086	-80.6715
CA-TPD	DBF	2012-2014	42.6353	-80.5577
DE-Hai	DBF	2000-2011	51.0792	10.4530
DE-Lnf	DBF	2003-2006, 2010-2012	51.3282	10.3678
DK-Sor	DBF	2000, 2002-2014	55.4859	11.6446
IT-CA3	DBF	2012-2014	42.3800	12.0222
IT-Col	DBF	2005-2014	41.8494	13.5881
IT-Isp	DBF	2013-2014	45.8126	8.6336
IT-PT1	DBF	2003-2004	45.2009	9.0610
IT-Ro1	DBF	2001-2008	42.4081	11.9300
IT-Ro2	DBF	2002-2008, 2010, 2012	42.3903	11.9209
JP-MBF	DBF	2004-2005	44.3869	142.3186
PA-SPn	DBF	2008	9.3181	-79.6346
US-MMS	DBF	2000-2014	39.3232	-86.4131
US-Oho	DBF	2004-2013	41.5545	-83.8438
US-UMB	DBF	2002-2014	45.5598	-84.7138
US-UMd	DBF	2008-2013	45.5625	-84.6975
US-WCr	DBF	2000-2006, 2011-2014	45.8059	-90.0799
ZM-Mon	DBF	2007-2008	-15.4378	23.2528
AU-Tum	EBF	2002-2014	-35.6566	148.1517
AU-Wac	EBF	2006-2008	-37.4259	145.1878
AU-Whr	EBF	2012-2014	-36.6732	145.0294

AU-Wom	EBF	2011-2014	-37.4222	144.0944
BR-Sa3	EBF	2001-2003	-3.0180	-54.9714
CN-Din	EBF	2003-2005	23.1733	112.5361
GF-Guy	EBF	2004-2014	5.2788	-52.9249
GH-Ank	EBF	2012, 2014	5.2685	-2.6942
IT-Cpz	EBF	2001-2008	41.7053	12.3761
MY-PSO	EBF	2003-2009	2.9730	102.3062
AU-ASM	ENF	2011-2014	-22.2830	133.2490
CA-NS1	ENF	2003-2004	55.8792	-98.4839
CA-NS2	ENF	2003-2004	55.9058	-98.5247
CA-NS3	ENF	2003-2004	55.9117	-98.3822
CA-NS4	ENF	2003-2004	55.9144	-98.3806
CA-Qfo	ENF	2004-2010	49.6925	-74.3421
CA-SF1	ENF	2004-2005	54.4850	-105.8176
CA-SF2	ENF	2002-2004	54.2539	-105.8775
CA-TP1	ENF	2003-2014	42.6609	-80.5595
CA-TP2	ENF	2003-2007	42.7744	-80.4588
CH-Dav	ENF	2007-2012, 2014	46.8153	9.8559
CN-Qia	ENF	2003-2005	26.7414	115.0581
CZ-BK1	ENF	2011-2013	49.5021	18.5369
DE-Lkb	ENF	2010-2013	49.0996	13.3047
DE-Obe	ENF	2010-2014	50.7867	13.7213
DE-Tha	ENF	2000-2014	50.9624	13.5652
FI-Hyy	ENF	2000-2002, 2004-2013	61.8474	24.2948
FI-Sod	ENF	2001-2006, 2011-2014	67.3624	26.6386
FR-LBr	ENF	2005-2008	44.7171	-0.7693
IT-Lav	ENF	2005-2014	45.9562	11.2813
IT-Ren	ENF	2002-2003, 2005-2014	46.5869	11.4337
IT-SR2	ENF	2014	43.7320	10.2910
IT-SRo	ENF	2003-2012	43.7279	10.2844
NL-Loo	ENF	2000-2014	52.1666	5.7436
RU-Fyo	ENF	2007-2014	56.4615	32.9221
US-Blo	ENF	2000-2006	38.8953	-120.6328
US-GLE	ENF	2005-2013	41.3665	-106.2399
US-Me2	ENF	2002-2014	44.4523	-121.5574
US-Me3	ENF	2004-2008	44.3154	-121.6078
US-Me5	ENF	2000-2002	44.4372	-121.5668
US-Me6	ENF	2011	44.3233	-121.6078
US-NR1	ENF	2002-2014	40.0329	-105.5464
AT-Neu	GRA	2003-2012	47.1167	11.3175
AU-DaP	GRA	2008-2012	-14.0633	131.3181
AU-Emr	GRA	2012-2013	-23.8587	148.4746
AU-Rig	GRA	2011-2014	-36.6499	145.5759
AU-Stp	GRA	2009-2014	-17.1507	133.3502

AU-Ync	GRA	2013-2014	-34.9893	146.2907
CH-Cha	GRA	2006-2014	47.2102	8.4104
CH-Fru	GRA	2006-2014	47.1158	8.5378
CH-Oe1	GRA	2003-2007	47.2858	7.7319
CN-Cng	GRA	2008-2009	44.5934	123.5092
CN-Dan	GRA	2004-2005	30.4978	91.0664
CN-HaM	GRA	2002-2004	37.3700	101.1800
CN-Sw2	GRA	2011	41.7902	111.8971
CZ-BK2	GRA	2007-2012	49.4944	18.5429
DE-Gri	GRA	2007-2014	50.9500	13.5126
DK-Eng	GRA	2006-2007	55.6905	12.1918
DK-ZaH	GRA	2001-2004	74.4733	-20.5503
IT-MBo	GRA	2005-2013	46.0147	11.0458
IT-Tor	GRA	2009-2014	45.8444	7.5781
NL-Hor	GRA	2007-2010	52.2404	5.0713
PA-SPs	GRA	2008-2009	9.3138	-79.6314
RU-Tks	GRA	2011-2013	71.5943	128.8878
US-AR1	GRA	2010-2012	36.4267	-99.4200
US-AR2	GRA	2010-2011	36.6358	-99.5975
US-Goo	GRA	2003-2006	34.2547	-89.8735
US-IB2	GRA	2005-2011	41.8406	-88.2410
US-SRG	GRA	2009-2014	31.7894	-110.8277
US-Var	GRA	2001-2014	38.4133	-120.9507
US-Wkg	GRA	2005-2014	31.7365	-109.9419
AR-SLu	MF	2010	-33.4648	-66.4598
BE-Vie	MF	2000-2014	50.3050	5.9981
CH-Lae	MF	2005-2014	47.4781	8.3650
CN-Cha	MF	2003-2005	42.4025	128.0958
JP-SMF	MF	2003-2006	35.2617	137.0788
US-PFa	MF	2000-2014	45.9459	-90.2723
US-Syv	MF	2002-2007, 2012-2014	46.2420	-89.3477
AU-TTE	SH	2013-2014	-22.2870	133.6400
CA-NS6	SH	2003-2004	55.9167	-98.9644
CA-NS7	SH	2003-2004	56.6358	-99.9483
CA-SF3	SH	2002-2005	54.0916	-106.0053
ES-Amo	SH	2008-2012	36.8336	-2.2523
ES-LgS	SH	2007	37.0979	-2.9658
ES-LJu	SH	2005-2013	36.9266	-2.7521
US-SRC	SH	2009-2013	31.9083	-110.8395
US-Sta	SH	2008	41.3966	-106.8024
US-Whs	SH	2008-2014	31.7438	-110.0522
AU-Cpr	SAV	2013-2014	-34.0021	140.5891
AU-DaS	SAV	2008-2014	-14.1593	131.3881
AU-Dry	SAV	2009-2014	-15.2588	132.3706

AU-GWW	SAV	2013-2014	-30.1913	120.6541
SD-Dem	SAV	2007-2009	13.2829	30.4783
SN-Dhr	SAV	2011-2013	15.4028	-15.4322
ZA-Kru	SAV	2001-2012	-25.0197	31.4969
AU-Fog	WET	2007	-12.5452	131.3072
CN-Ha2	WET	2003-2005	37.6086	101.3269
FI-Lom	WET	2008-2009	67.9972	24.2092
AU-Ade	WSA	2008	-13.0769	131.1178
AU-Gin	WSA	2012-2014	-31.3764	115.7138
AU-How	WSA	2004-2014	-12.4943	131.1523
AU-RDF	WSA	2012	-14.5636	132.4776
US-SRM	WSA	2004-2014	31.8214	-110.8661
US-Ton	WSA	2002-2014	38.4316	-120.9660

2. Description of key modules in BEPS

2.1 Leaf-level photosynthesis and transpiration

BEPS adopts the Farquhar model (Farquhar et al., 1980) to calculate the leaf-level photosynthetic rate, expressed as:

$$A = \min(W_c, W_j) - R_d \quad (1.)$$

where W_c is the photosynthetic rate (μmol m^{-2} s^{-1}) under RuBP carboxylase/oxygenase limited conditions, W_j is the photosynthetic rate under electron transport limited conditions in the RuBP regeneration process, and R_d is the dark respiration rate. W_c, W_j, and R_d are calculated as:

$$W_c = V_{cmax}\frac{C_i - \Gamma}{C_i + K} \quad (2.)$$

$$W_j = J\frac{C_i - \Gamma}{4C_i + 8K} \quad (3.)$$

$$R_d = 0.015V_{cmax} \quad (4.)$$

where V_{cmax} is the maximum carboxylation rate (μmol m^{-2} s^{-1}) calculated from preset V_{cmax}^{25} and a temperature dependent function (Sharkey et al., 2007), J is the electron transport rate (μmol m^{-2} s^{-1}), C_i is the intercellular CO_2 concentration (μmol mol^{-1}), Γ is the CO_2 compensation point without dark respiration (μmol mol^{-1}), and K is a Rubisco enzyme kinetics function as $K = K_c/(1 + O_i/K_o)$. K_c, K_o are Michaelis-Menten constants for CO_2 (μmol mol^{-1}) and O_2 (mmol mol^{-1}), and O_i is the intercellular oxygen concentration (mmol

mol^{-1}). J is a function of PPFD (μmol m^{-2} s^{-1}) and the maximum electron transport rate (J_{max}), expressed as:

$$J = J_{max} \times \frac{PPFD}{PPFD + 2.1J_{max}} \quad (5.)$$

and J_{max} is obtained using the equation by Medlyn et al. (1999):

$$J_{max} = 2.39V_{cmax} - 14.2 \quad (6.)$$

BEPS solves the A and g_s using the cubic analytical method (Baldocchi, 1994) by coupling the Farquhar model and the Ball-Woodrow-Berry model (Ball et al., 1987), which is expressed as:

$$g_s = m \cdot A\frac{RH}{C_a} + g_0 \quad (7.)$$

where A is the photosynthetic rate (mol m^{-2} s^{-1}), RH is the relative humidity at the leaf surface (%), C_a is the CO_2 concentration at the leaf surface (μmol mol^{-1}), m is the slope of linear regression between g_s and $A \cdot RH/C_a$ (unitless), and g_0 is the intercept of the regression representing minimum g_s. The leaf-level transpiration is then calculated by applying the Penman-Monteith equation:

$$T = \frac{\Delta(\mathrm{R_n} - G) + \rho c_p VPD g_b}{\lambda\left(\Delta + \left(1 + \frac{g_b}{g_s}\right)\gamma\right)} \quad (8.)$$

where R_n is the net radiation on the leaf surface (W m^{-2}), G is the heat storage of the leaf, ρ is the density of air (kg m^{-3}), c_p is the specific heat of air (J kg^{-1} °C^{-1}), VPD is the vapor pressure deficit on the leaf surface (kPa), Δ is the rate of change of saturation specific humidity with air temperature (kPa °C^{-1}), λ is the latent heat of water (J kg^{-1}), γ is the psychrometric constant (kPa °C^{-1}), and g_b is the leaf boundary layer resistance to water vapor (m s^{-1}).

2.2 Two-level scheme upscaling carbon and water fluxes from leaf to canopy

The canopy can be separated into sunlit and shaded leaf groups based on the first order of the incoming solar radiation on leaves (Chen et al., 1997; Norman, 1982). Sunlit leaves receive both direct and diffuse radiation and shaded leaves only receive diffuse solar radiation. Sunlit and shaded LAI (LAI_{sunlit} and LAI_{shaded}) are calculated in BEPS following the method described in Chen et al. (1999):

$$LAI_{sunlit} = 2cos\theta\left(1 - e^{-\frac{0.5\Omega LAI_{total}}{cos\theta}}\right) \quad (9.)$$

$$LAI_{shaded} = LAI_{total} - LAI_{sunlit} \quad (10.)$$

where θ is the solar zenith angle, LAI_{total} is the total leaf area index of the canopy, and Ω is the clumping index. The leaf-level A and T are then upscaled to the canopy level (GPP, T_{total}):

$$GPP = A_{sunlit} \times LAI_{sunlit} + A_{shaded} \times LAI_{shaded} \quad (11.)$$

$$T_{total} = T_{sunlit} \times LAI_{sunlit} + T_{shaded} \times LAI_{shaded} \quad (12.)$$

where A_{sunlit} and T_{sunlit} are the instantaneous photosynthetic rate and the transpiration from a sunlit leaf, A_{shaded} and T_{shaded} are the instantaneous photosynthetic rate and the transpiration from a shaded leaf. BEPS also simulates evaporation from soil (E_{soil}) and from wet leaf surface (E_{leaf}):

$$ET = T_{total} + E_{soil} + E_{leaf} \quad (13.)$$

but these two processes, E_{soil} and E_{leaf}, are not regulated by stomatal functions and leaf photosynthesis, thus not likely to change much in m and V_{cmax} optimizations.

3. The parameter optimization algorithm to estimate m and V_{cmax}^{25} in BEPS

The Bayesian parameter optimization has been tested with good accuracy and high efficiency for m and V_{cmax25} retrievals in Leng et al. (2024a). With optimized seasonally varied m and V_{cmax}^{25}, the estimates of carbon and water fluxes can be significantly improved. In this study, the carbon-water-coupling cost function was adopted to derive m and V_{cmax}^{25} at site for each month, which is expressed as:

$$f_{cost} = |1 - a_{GPP_{obs}}^{GPP_{mod}}| \times \frac{1}{N}\sum\left(\frac{GPP_{mod} - GPP_{obs}}{GPP_{obs}}\right)^2 + |1 - a_{ET_{obs}}^{ET_{mod}}| \times \frac{1}{N}\sum\left(\frac{ET_{mod} - ET_{obs}}{ET_{obs}}\right)^2 \quad (14.)$$

where GPP_{obs} is the observed GPP from fluxes, GPP_{mod} is the modeled GPP from BEPS, ET_{obs} is the observed ET from fluxes, ET_{mod} is the modeled ET from BEPS, N is the total number of hourly simulations in a parameter optimization interval, $a_{GPP_{obs}}^{GPP_{mod}}$ is the ordinal

least square regression (OLS) slope between GPP_{mod} and GPP_{obs}, $a_{ET_{obs}}^{ET_{mod}}$ is the OLS slope between ET_{mod} and ET_{obs}.

At site level, m and V_{cmax25} were estimated monthly by minimizing the cost function, in which m was set in range [0, 25] and V_{cmax25} was set in range [10, 200] according to the reported ranges in literature, and the optimized m and V_{cmax25} were filtered based on the normal ranges reported in literature, respectively. (Chen et al., 2022; Miner et al., 2017; Smith et al., 2019; Wolz et al., 2017). BEPS was run for 500 times for m and V_{cmax25} of each month at each site to get the global optima in the Bayesian parameter optimization.

3. Global distributions and seasonal variations of m and V_{cmax}

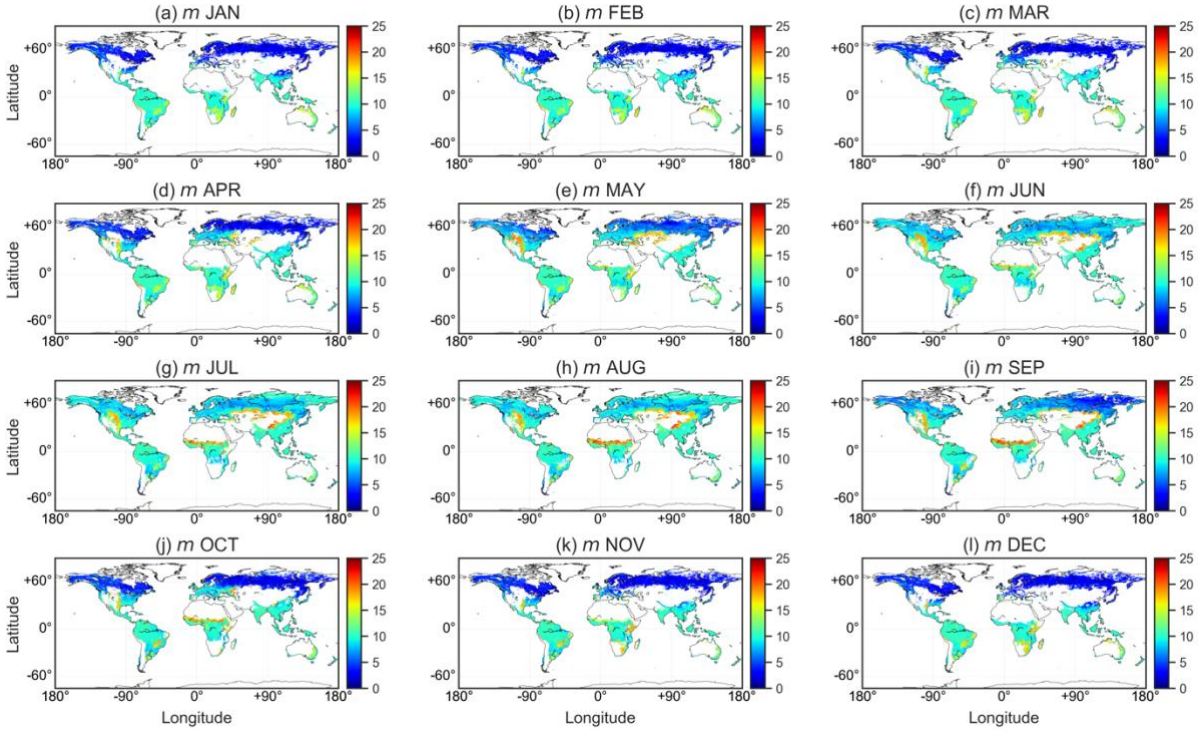

Figure S1. Monthly spatial patterns of global m during 2001-2020. (a) – (l) averaged from January to December, respectively. Courtesy of Leng et al. (2024b).

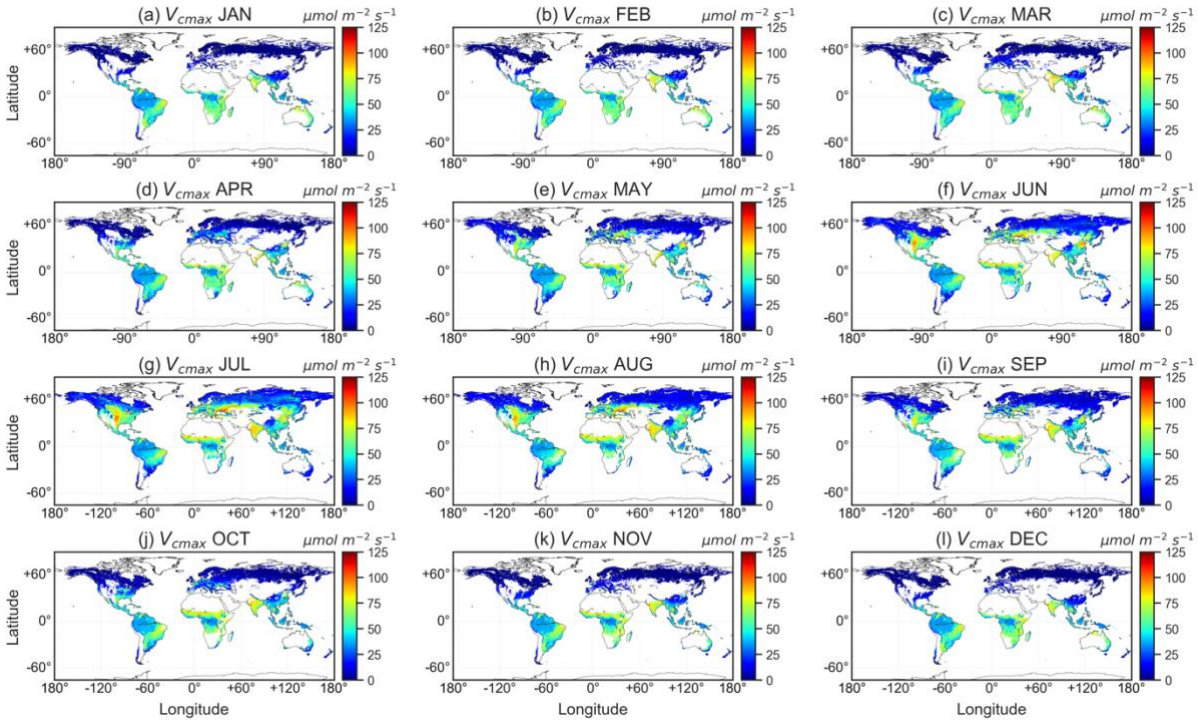

Figure S2. Monthly spatial patterns of global V_{cmax} during 2001-2020. (a) – (l) averaged from January to December, respectively. Courtesy of Leng et al. (2024b).

The monthly spatial patterns of global m and V_{cmax} during 2001-2020 in Figure S1 and Figure S2, respectively. Strong seasonal variations in m and V_{cmax} are observed in boreal regions while m and V_{cmax} in subtropical and tropical regions are fairly constant within a year.

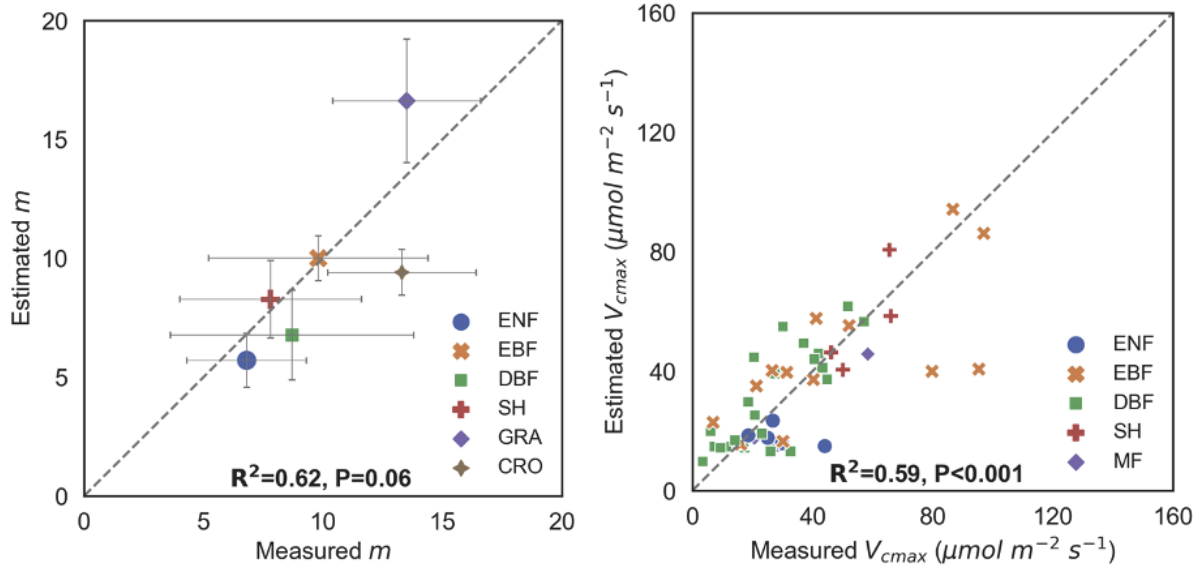

Figure S3. Left: Comparison between the PFT-scale mean values of estimated m from the Random Forest regressor and the measured m values reported in the review by Miner et al. (2017). Each horizontal and vertical bar represents the mean m ± 1 standard deviation in the

literature values and the estimated values, respectively. The sample sizes of measured m for each PFT are n = 23 (ENF), n = 23 (EBF), n = 54 (DBF), n = 11 (SH), n = 5 (GRA), and n = 53 (CRO). Right: Comparison between the PFT-scale mean values of predicted V_{cmax} from the Random Forest regressor and the measured V_{cmax} values reported in the review by Smith et al. (2019). Courtesy of Leng et al. (2024b).

To further validate the gridded global m and V_{cmax}, we compared the global retrievals of m and V_{cmax} in this study with the m census for various biomes from the review by Miner et al. (2017) and the V_{cmax} field measurements collected from Smith et al. (2019), as shown in Figure S3. m estimates in this study were compared with the mean and standard deviation in Miner et al. (2017) while V_{cmax} observations with the timestamp of measurement were compared with the estimated V_{cmax} in the corresponding time period in 2001-2020. Only 0.25° pixels with more than three V_{cmax} measurements were selected in the comparison. The estimated m in the global retrievals agrees well with the measured m, with $R^2 = 0.62$ ($P = 0.06$) and the estimated V_{cmax} in the global retrievals agrees well with the measured V_{cmax}, with $R^2 = 0.59$ ($P < 0.001$).

References

Baldocchi, D. (1994). An analytical solution for coupled leaf photosynthesis and stomatal conductance models. *Tree Physiology, 14*, 1069-1079

Ball, J.T., Woodrow, I.E., & Berry, J.A. (1987). A Model Predicting Stomatal Conductance and its Contribution to the Control of Photosynthesis under Different Environmental Conditions. In J. Biggins (Ed.), *Progress in Photosynthesis Research: Volume 4 Proceedings of the VIIth International Congress on Photosynthesis Providence, Rhode Island, USA, August 10–15, 1986* (pp. 221-224). Dordrecht: Springer Netherlands

Chen, J., Wang, R., Liu, Y., He, L., Croft, H., Luo, X., Wang, H., Smith, N., Keenan, T., Prentice, I., Zhang, Y., Ju, W., & Dong, N. (2022). Global datasets of leaf photosynthetic capacity for ecological and earth system research. *Earth System Science Data, 14*, 4077-4093

Chen, J.M., Liu, J., Cihlar, J., & Goulden, M.L. (1999). Daily canopy photosynthesis model through temporal and spatial scaling for remote sensing applications. *Ecological Modelling, 124*, 99-119

Chen, J.M., Rich, P.M., Gower, S.T., Norman, J.M., & Plummer, S. (1997). Leaf area index of boreal forests: Theory, techniques, and measurements. *Journal of Geophysical Research: Atmospheres, 102*, 29429-29443

Farquhar, G.D., von Caemmerer, S., & Berry, J.A. (1980). A biochemical model of photosynthetic CO2 assimilation in leaves of C3 species. *Planta, 149*, 78-90

Leng, J., Chen, J.M., Li, W., Luo, X., Rogers, C., Croft, H., Xie, X., Staebler, R.M. (2024a). Optimizing seasonally variable photosynthetic parameters based on joint carbon and water flux constraints. Preprint at Research Square, https://doi.org/10.21203/rs.3.rs-3832505/v1

Leng, J., Chen, J.M., Li, W., Luo, X., Xu, M., Rogers, C., Yan, Y. (2024b). Declining global sensitivity of photosynthesis to stomatal conductance. Preprint at Research Square, https://doi.org/10.21203/rs.3.rs-3832529/v1

Medlyn, B.E., Badeck, F.W., De Pury, D.G.G., Barton, C.V.M., Broadmeadow, M., Ceulemans, R., De Angelis, P., Forstreuter, M., Jach, M.E., Kellomäki, S., Laitat, E., Marek, M., Philippot, S., Rey, A., Strassemeyer, J., Laitinen, K., Liozon, R., Portier, B., Roberntz, P., Wang, K., & Jstbid, P.G. (1999). Effects of elevated [CO2] on photosynthesis in European forest species: a meta-analysis of model parameters. *Plant, Cell & Environment, 22*, 1475-1495

Miner, G.L., Bauerle, W.L., & Baldocchi, D.D. (2017). Estimating the sensitivity of stomatal conductance to photosynthesis: a review. *Plant, Cell & Environment, 40*, 1214-1238

Norman, J.M. (1982). Simulation of Microclimates. In J.L. Hatfield, & I.J. Thomason (Eds.), *Biometeorology in Integrated Pest Management* (pp. 65-99): Academic Press

Sharkey, T.D., Bernacchi, C.J., Farquhar, G.D., & Singsaas, E.L. (2007). Fitting photosynthetic carbon dioxide response curves for C3 leaves. *Plant, Cell & Environment, 30*, 1035-1040

Smith, N.G., Keenan, T.F., Colin Prentice, I., Wang, H., Wright, I.J., Niinemets, U., Crous, K.Y., Domingues, T.F., Guerrieri, R., Yoko Ishida, F., Kattge, J., Kruger, E.L., Maire, V., Rogers, A., Serbin, S.P., Tarvainen, L., Togashi, H.F., Townsend, P.A., Wang, M., Weerasinghe, L.K., & Zhou, S.X. (2019). Global photosynthetic capacity is optimized to the environment. *Ecological Letter, 22*, 506-517

Wolz, K.J., Wertin, T.M., Abordo, M., Wang, D., & Leakey, A.D.B. (2017). Diversity in stomatal function is integral to modelling plant carbon and water fluxes. *Nature Ecology & Evolution, 1*, 1292-1298